EurJIC
European Journal of Inorganic Chemistry

Research Article
doi.org/10.1002/ejic.202200319

Chemistry Europe
European Chemical Societies Publishing

www.eurjic.org

Mixed Valency vs Radical Bridge Formulation in Symmetrically and Asymmetrically Ligated Diruthenium Complexes

Sudipta Mondal,[a] Brigitte Schwederski,[a] Stanislav Záliš,[b] and Wolfgang Kaim*[a]

This manuscript is dedicated to Prof. Dr. Wolfgang Beck on the occasion of his 90th birthday.

The asymmetrical dinuclear [{(trpy*)Ru}$_2$(μ-adc-Salph)Cl](PF$_6$) **1**(PF$_6$), trpy* = 4,4′,4″-tri-*tert*-butyl-2,6,2′,6″-terpyridine, adc-Salph = 1-benzoyl-2-salicyloylhydrazido(3-), and the related symmetrical dinuclear [{Cl(trpy*)Ru}$_2$(μ,η^2:η^2-adc-Ph)](PF$_6$) **2**(PF$_6$), adc-Ph = 1,2-bis(benzoyl)hydrazido(2-), were synthesized and structurally characterized. Both paramagnetic compounds were compared with the previously reported symmetrical [{(trpy*)Ru}$_2$(μ,η^3:η^3-adc-Sal)](PF$_6$) **3**(PF$_6$) containing the bis-tridentate bridge 1,2-bis(salicyloyl)hydrazido(4-). Molecular structures and magnetic resonance features (^{1}H NMR, EPR) indicate spin density distribution over the metal(s) and the bridging ligand. Reversible one-electron reduction and oxidation were possible in all instances yielding comproportionation constants K_c of about 10^9 for the paramagnetic intermediates **1**$^+$–**3**$^+$. Structural results, spin density distribution and UV-Vis-NIR spectroelectrochemistry were analyzed for **1**$^+$ with the help of TD-DFT calculations for a model compound (*tert*-Bu→Me). Intense absorptions around λ_{max} = 1450–1650 nm for the cations were assigned to mixed metal/ligand transitions with significant inter-valence charge transfer (IVCT) character. For both the symmetrical and asymmetrical arrangements the cationic intermediates can be described as considerably mixed metal/ligand systems.

Introduction

Mixed-valent (MV) dinuclear complexes with low spin d^5/d^6 configuration, especially Ru^{III}Ru^{II} combinations, have served well as models in the study of intramolecular electron transfer processes.[1,2] While many symmetrical[3,4] complexes have been investigated, the asymmetrical analogues are equally important because electron transfer-active biological systems are typically asymmetrical.[2] For instance, cyclometalated as well as non-cyclometalated asymmetrical diruthenium systems have been described.[5–9] The focus of the present study is on non-cyclometalated diruthenium systems; few such examples[9] are known which exhibit strong ($\varepsilon \approx 5000$ M^{-1} cm^{-1}) NIR absorption, an important feature for potential applications.[10]

Symmetrical 1,2-dicarbonylhydrazido(2-) (adc-R(2-)) ligands have shown their ability in establishing efficient electronic communication between two metal centres in diruthenium complexes.[11–13] For these donor ligands, the metal-ligand-metal electronic interaction can be understood by a super-exchange mechanism in terms of *hole transfer*.[3,12] The potential of a related *asymmetrical* bridging ligand, designated as adc-Salph(3-) (Scheme 1), will be presented here. This ligand has the ability to coordinate two metal centres in a μ-η^2:η^3 fashion (N,O/O,N,O′) which has been used to prepare supramolecular complexes like metallacrowns.[14] Therefore, complexes with this kind of bridging ligand with an odd number of donor sites would be interesting from a structural point of view. A few other polynuclear complexes of adc-Salph(3-) or related adc-R ligands have been reported,[15,16] but dinuclear complexes are rare and have not been studied electrochemically or with respect to mixed-valency.

The asymmetrical complex **1**(PF$_6$) (Scheme 2) containing adc-Salph(3-) has been studied structurally, electrochemically and spectroscopically (EPR, NMR, UV-Vis-NIR), and the results

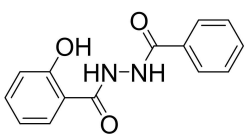

1-benzoyl-2-salicyloylhydrazine
H_3adc-Salph

Scheme 1. Protonated form of the ligand adc-Salph(3-).

[a] *Dr. S. Mondal, Dr. B. Schwederski, Prof. Dr. W. Kaim*
Institut für Anorganische Chemie,
Universität Stuttgart,
Pfaffenwaldring 55,
D-70550 Stuttgart, Germany
E-mail: kaim@iac.uni-stuttgart.de
http://www.iac.uni-stuttgart.de/Arbeitskreise/AkKaim/index.html
[b] *Dr. S. Záliš*
The Czech Academy of Sciences,
J. Heyrovský Institute of Physical Chemistry,
Dolejškova 3, 18223
Prague, Czech Republic

Supporting information for this article is available on the WWW under https://doi.org/10.1002/ejic.202200319

Research Article
doi.org/10.1002/ejic.202200319

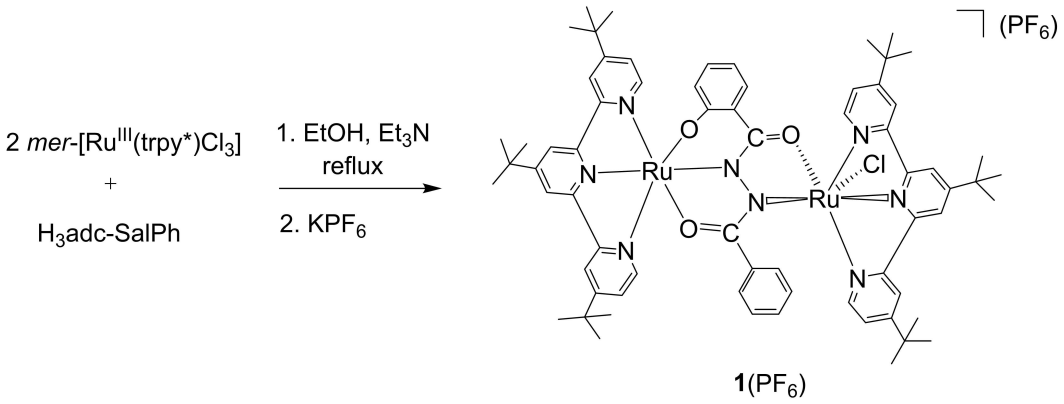

Scheme 2. Reaction scheme for **1**(PF_6).

can be compared to those from the symmetrical analogues **2**(PF_6) and **3**(PF_6)[17] in Scheme 3. The co-ligand trpy* has been chosen because of its meridional coordination, moderate π acceptor strength and its ability to ensure solubility in aprotic media; for the TD-DFT calculations employed here the *tert*-butyl groups in trpy* were replaced by methyl (→trpy′).

For comparison with the asymmetrical system **1**^{n} we have prepared and studied the new species **2**(PF_6), containing two equivalent chlororuthenium sites. The symmetrical **3**^{n} with bis-tridentate 1,2-bis(salicyloyl)hydrazido(4-) has also been utilized for comparison, its investigation was reported earlier.[17]

Results and Discussion

Reaction of H_3adc-Salph[14] (Scheme 1) with two equivalents of *mer*-[Ru(trpy*)Cl_3][18] in the presence of triethylamine as a base in refluxing ethanol resulted in the asymmetric complex, [{(trpy*)Ru}$_2$(μ-adc-Salph)Cl](PF_6), **1**(PF_6). The cation/anion ratio (1:1) is in agreement with results from elemental analysis and mass spectrometry. This ratio suggests the formal presence of Ru^{II} and Ru^{III} centres in **1**(PF_6), resulting in a paramagnetic complex, as evident from ^{1}H NMR (Figure 1 and Figure S1) and EPR spectroscopy (see below). Paramagnetism with variable metal/ligand spin distribution may cause considerable shifts and line broadening which can preclude satisfactory NMR analysis. The bidentate/tridentate ligand adc-Salph(3-) is interacting with two different ruthenium complex fragments and thus results in different configurations A and B (Scheme 4) in the complex. Meridional coordination of trpy* and the N,O donor combination from the bridging ligand gives rise to two alternatives, B1 and B2, which results in different constitutional isomers; these were named as A/B1 and A/B2 according to the different combinations.

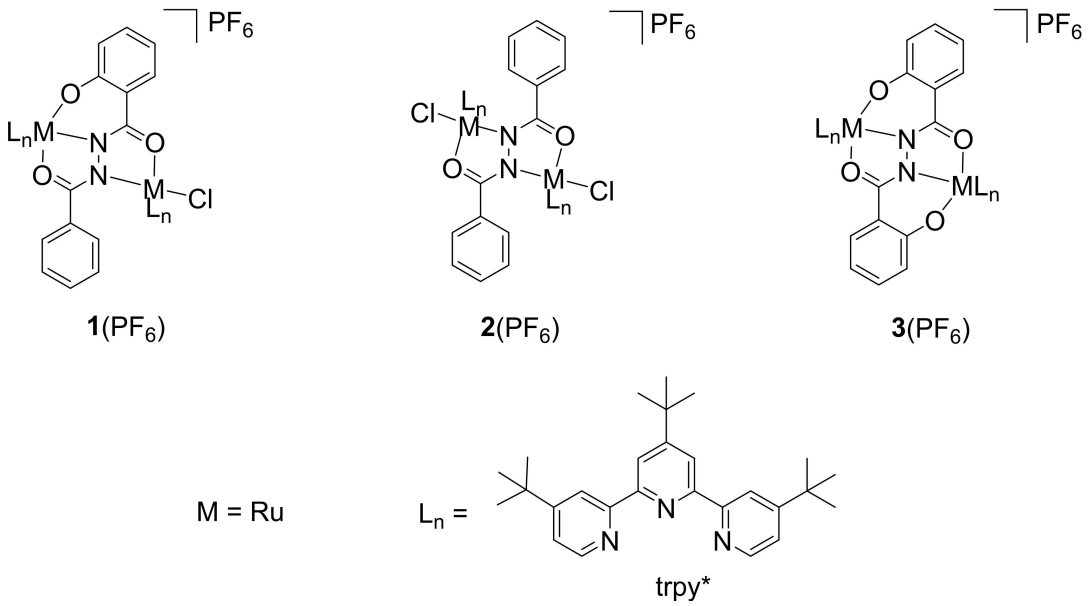

Scheme 3. Symmetrical and asymmetrical complexes of 1,2-dicarbonylhydrazido(2-)-type ligands with different aryl substituents.

Research Article
doi.org/10.1002/ejic.202200319

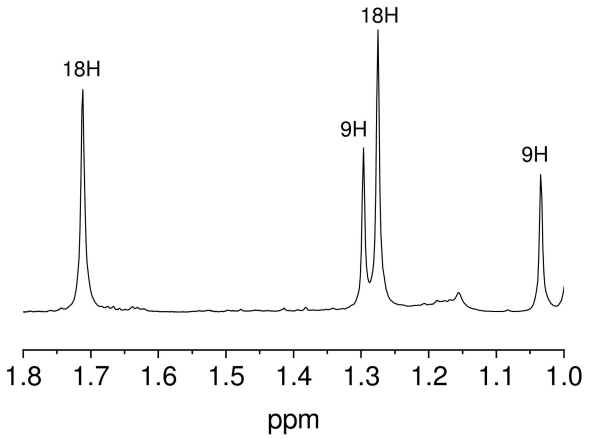

Figure 1. ^{1}H NMR resonances (only *tert*-butyl protons) of **1**(PF_6) in $(CD_3)_2CO$. Solvent impurity at 1.15 ppm, spectrum with $\delta > 4$ ppm shown in Figure S1.

The reaction procedure and the chemical structure depicting the A/B2 isomer for **1**(PF_6) have been summarized in Scheme 2. Structural characterization (see below) has confirmed the formation of the isomer A/B2 (Scheme 4) where the chloride function is ligated *trans* to an N_{azo} atom. The new paramagnetic bis(chlororuthenium) compound **2**(PF_6) has been prepared via a conventional route[11–13,19] as symmetrical analogue of **1**(PF_6) (Figure S2, Tables S1, S3). Its ^{1}H NMR spectrum confirms symmetry and paramagnetism through shifted resonances (Exp. Section). The symmetrical complexes [{Cl(trpy*)Ru}$_2$(μ,η^2:η^2-adc-Ph)](PF_6), **2**(PF_6), and [{(trpy*)Ru}$_2$(μ,η^3:η^3-adc-Sal)](PF_6), **3**(PF_6),[17] exhibit two singlets for the *tert*-butyl protons from trpy* in their ^{1}H NMR spectra. They appear in the alkane region between 1.3 and 1.9 ppm; one singlet corresponds to nine protons from the *tert*-butyl group connected to the central pyridyl ring and the other to 18 protons from those connected to the terminal pyridyl rings. In contrast, four signals between 1.0 and 1.8 ppm were observed for **1**(PF_6), as depicted in Figure 1. The different coordinative environment of trpy* in A and B2 and a non-uniform charge and spin density distribution over both ruthenium complex fragments, induced by the asymmetrical ligand coordination, are held responsible.

Molecular structure analyses

Single crystals appropriate for X-ray diffraction were grown by slow diffusion of hexane into a 1,2-dichloroethane solution of **1**(PF_6). The asymmetrical complex **1**(PF_6) crystallizes in the space group *Pbca* (Table S1) and the molecular structure is shown in Figure 2, top. Crystallographic data are listed in Table S1 and selected bond lengths and angles are summarized in Table 1 and Tables S2. For comparison to **1**(PF_6), CCDC 2150605, Table 1 contains relevant data for the symmetrical analogues **2**(PF_6), CCDC 2150606, and **3**(PF_6)[17] (Scheme 3) with chloro- and phenolato-coordinated ruthenium, respectively (cf. below for discussion).

Structural information like the N–N bond distance is important for characterising "odd-electron" mono- or dinuclear complexes with azo-containing redox-active ligands.[20,21] Structural information can also be an additional support along with widely used NIR-band-analysis in characterizing diruthenium mixed-valent species. Especially when communicating ruthenium fragments are in different environments, structural data can play a pivotal role in establishing the proper mixed-valence

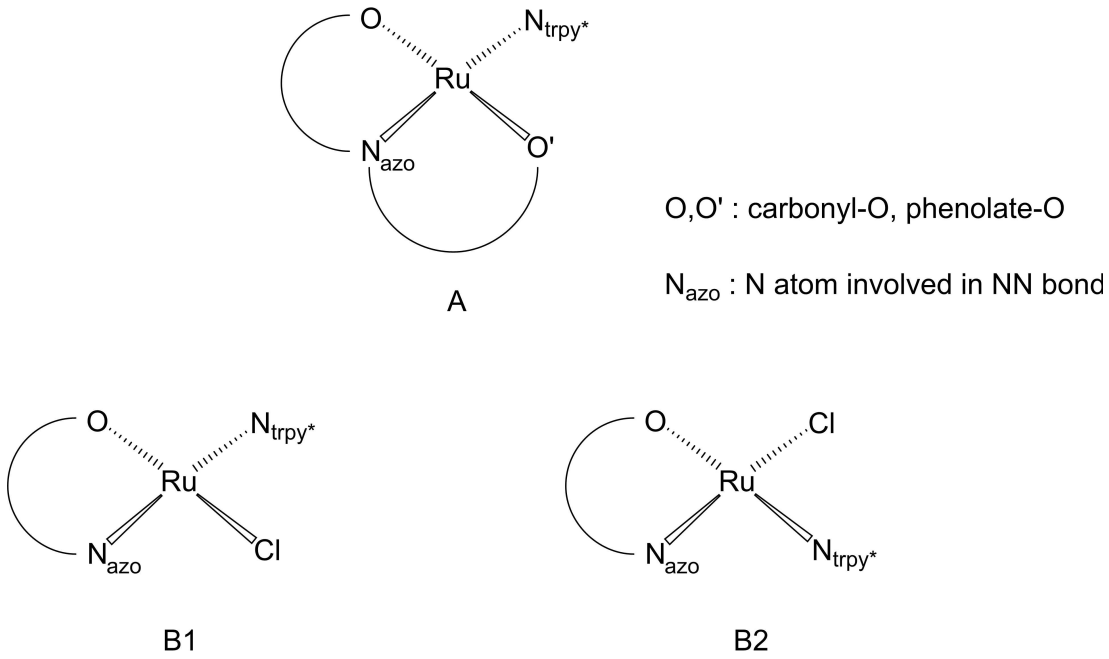

Scheme 4. Coordination environments (only equatorial positions shown in an octahedral geometry involving *mer*-trpy*) of different molecular parts of the complex cation **1**$^+$.

Research Article
doi.org/10.1002/ejic.202200319

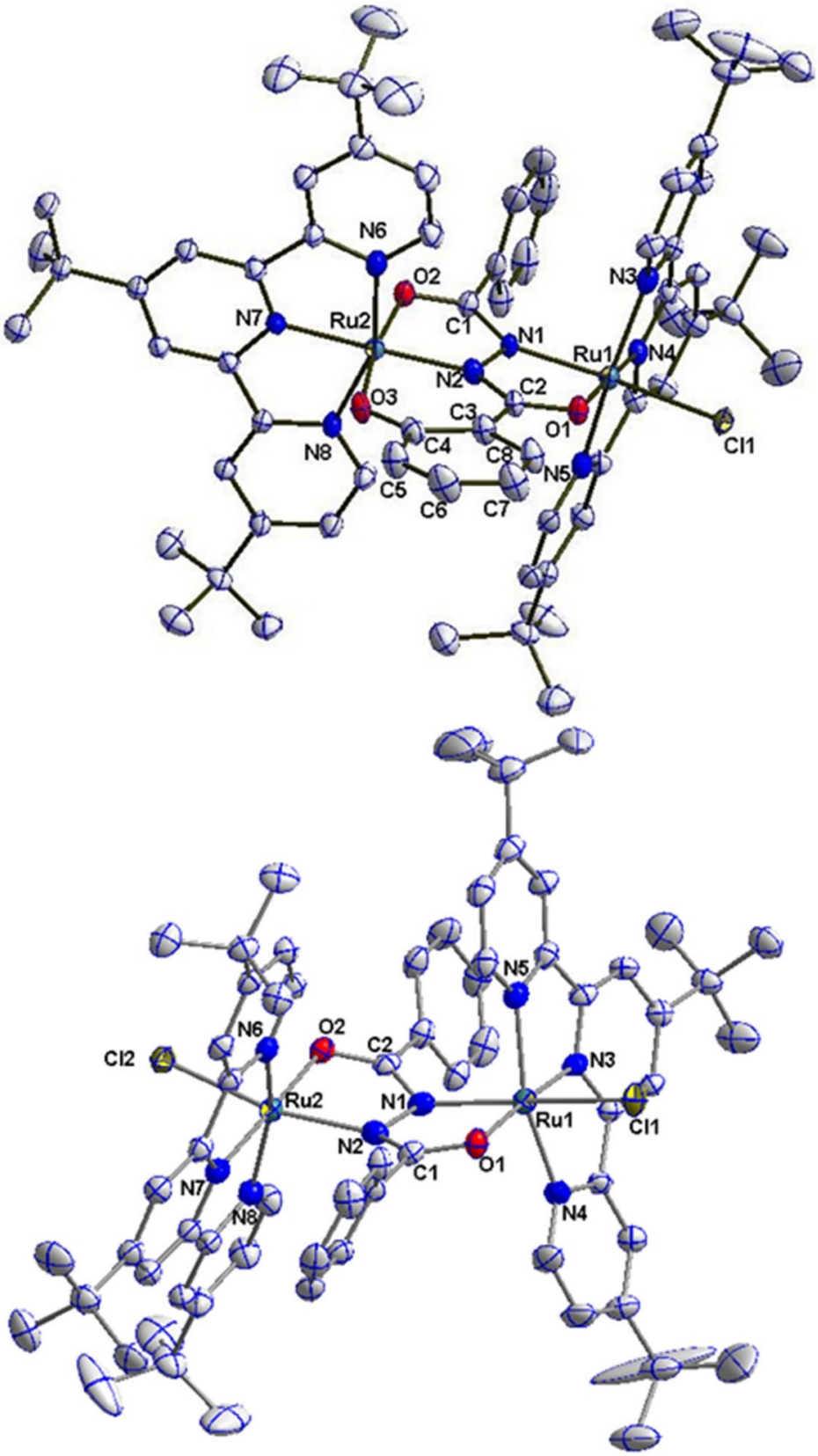

Figure 2. (Top) Molecular structure of the cation in the crystal of **1**$(PF_6)\times C_2H_4Cl_2$. (Bottom) Molecular structure of the cation in the crystal of **2**(PF_6). Thermal ellipsoids are given at the 50% probability level; H atoms are removed for clarity.

assignment. T. J. Meyer and co-workers have thus presented one symmetrical mixed-valent compound $[Cl_3Ru(tppz)RuCl_3]^-$ (tppz = 2,3,5,6-tetrakis(2-pyridyl)pyrazine) for which the structural characterization helped to assign a Class II–III mixed-valence nature.[22]

The molecular structure of **1**(PF_6) clearly confirms the formation of the A/B2 constitutional isomer (Scheme 4) as mentioned previously. In the molecular region A, one ruthenium ion (Ru2 in Figure 2) is coordinated with trpy* and with the O2, N2 and O3 donor atoms of the bridging ligand in a bis-meridional fashion, forming four five-membered chelate rings and one six-membered chelate ring. On the other hand, in the molecular half B2 the chloride-binding ruthenium ion (Ru1 in Figure 2) is surrounded by three five-membered chelate rings. The molecular structure also depicts a π-π interaction between the phenyl ring from the bridging ligand and the central pyridyl ring from trpy*. The distance between the centroids of the two rings is 3.527 Å.

Three limiting electronic descriptions including mixed-valence (I), II)) and radical-bridged situations (III)) are possible for $\mathbf{1}^+$:

I) $[(trpy^*)Ru^{II}(\mu\text{-adc-Salph})^{3-}Ru^{III}(trpy^*)Cl]^+$
II) $[(trpy^*)Ru^{III}(\mu\text{-adc-Salph})^{3-}Ru^{II}(trpy^*)Cl]^+$
III) $[(trpy^*)Ru^{II}(\mu\text{-adc-Salph})^{2\bullet-}Ru^{II}(trpy^*)Cl]^+$

A valence delocalized ($Ru^{2.5}$–$Ru^{2.5}$) description is questionable here because, even in the case of strong interaction between the two metal centres, there should be a residual charge difference since the coordination environments of the two metal centres are significantly different. In addition, the Ru–$N_{adc\text{-}Salph}$ bonds, which could be an important structural marker in proposing a proper MV description, should differ in the molecular sections A and B2. The Ru–N_{trpy*} and Ru–$N_{adc\text{-}Salph}$ bond lengths are indeed considerably different (Table 1). In particular, the Ru–$N_{adc\text{-}Salph}$ (Ru2–N2) bond is significantly shorter at 1.968(4) Å than the Ru–N_{adcSal} distance of 1.990(4) Å in the symmetrical MV complex **3**(PF_6). The coordination environment surrounding ruthenium in this symmetrical complex resembles the molecular half A, and the complex **3**(PF_6) has been described as a resonance hybrid, $Ru^{2.5}(adc\text{-}Sal)^{4-}Ru^{2.5}$–$Ru^{II}(adc\text{-}Sal)^{3\cdot-}Ru^{II}$.[17] An assumption can be made, based on this analogy, that section A contains a Ru^{III} ion in **1**(PF_6), resulting in an electronic situation $[(trpy^*)Ru^{III}(adc\text{-}Salph)^{3-}Ru^{II}(trpy^*)Cl]^+$ (case II)). This assumption is also in agreement with the stronger donor ability of the phenolate function as compared to chloride, i.e. the phenolate coordinated ruthenium fragment will prefer the formally higher charge.

The third electronic description (case III)), which is a radical bridged situation, can be neglected here because the N–N distance of 1.427(6) Å suggests a single bond.[21] Noticeably, the C3–C4 bond length at 1.426(8) Å exhibits a slightly greater value when compared to other C–C distances in the salicyloyl ring. The C5–C6 and C7–C8 distances especially exhibit lower values (≈1.36 Å) than the standard aromatic C–C distance of 1.39 Å. These results along with other bond parameters (C–O/C–N distances) from the bridging ligand (Table 1) point to different resonance structures A to E (Scheme 5) of adc-Salph(3-), combining a hydrazido(2-) and a phenolate function. Specifically, D is expected to have a significant contribution in agreement with the C–O distances d_{C1-O2} = 1.293(6) Å and d_{C2-O1} = 1.274(6) Å from the OCNNCO core.

Table 1. Comparison of selected bond lengths (in Å) for the complexes from Scheme 3.

bond	**1**(PF_6)[a]	**2**(PF_6)	**3**(PF_6)[b]
Ru–N[c]	2.041(4)	2.051(3)	1.990(4)
	1.968(4)[d]	2.057(3)	1.990(4)
Ru–O[e]	2.046(4)	2.037(3)	2.054(4)
	2.074(4)	2.053(3)	2.038(4)
Ru–Cl	2.387(13)	2.3623(10)	–
	–	2.3770(10)	–
N–N	1.427(6)	1.437(4)	1.392(6)
C–O[f]	1.293(6)	1.270(5)	1.305(6)
	1.274(6)[d]	1.276(5)	1.304(6)

[a] For **1**(PF_6)×(1,2-$C_2H_4Cl_2$). [b] From ref. [17]. [c] Ru–N bonds to bridging ligand. [d] RuCl centre. [e] Ru–O bonds to bridging ligand. [f] Carbonyl function connected to NN

The symmetrical bis(chlororuthenium) compound **2**(PF_6) reveals a typical[13,21] molecular structure of the paramagnetic cation.[13] The *mer* coordination mode of the *tert*-butylated terpy ligand creates a configuration with chloride ligands in maximum (*trans*) distance to each other. The „S conformation"[21b] of the core in $\mathbf{2}^+$ with d(Ru···Ru) = 4.851 Å is similar to that observed in related cases.[13,21] The crucial N–N distance at 1.437(4) Å reflects a significant albeit not complete reduction of the bridging ligand which leaves some charge on the metals in agreement with a notable mixed valency.

Comparing the three paramagnetic diruthenium systems in Table 1 (see also Scheme 3) the Ru–N bond lengths are most indicative of the symmetry. Complex **2**(PF_6) with longer bonds and compound **3**(PF_6) with somewhat shorter Ru–N distances are clearly symmetrical whereas **1**(PF_6) reveals distinct asymmetry with one long and one short such parameter, differing by 0.073(4) Å. Experimental selected bond lengths and angles of $\mathbf{1}^+$ and DFT calculated bonding parameters of $\mathbf{1}^0$ and $\mathbf{1}^+$ for the trimethyl-terpyridine model are listed in Table S4. The calculated bonding parameters agree with the experiment except for the Ru1–N1 bond length which is overestimated by 0.037 Å. The experimental Ru1-Ru2 distance of 4.810 Å is well reproduced by the calculated value of 4.783 Å.

EPR spectroscopy

The paramagnetic nature of the isolated complex **1**(PF_6) is reflected by its considerably shifted ^{1}H NMR signals (Figure S1). Resonances related to the "aromatic" protons of **1**(PF_6) and **2**(PF_6) were found up to +21 ppm (Exp. Section).

DFT calculated spin densities for the trimethyl-terpyridine model of the radical cation $\mathbf{1}^+$ are listed in Table S5 and depicted in Figure 4. The spin is partly localized at one of the Ru centres and calculations give an asymmetric spin distribution of 0.05, 0.63 and 0.3 on Ru2, Ru1 and the μ-adc-Ph bridge, respectively.

Research Article
doi.org/10.1002/ejic.202200319

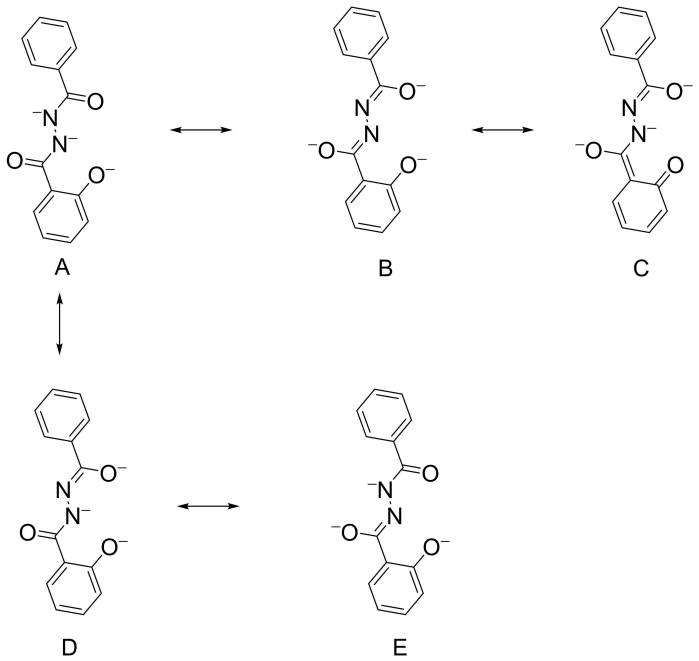

Scheme 5. Different resonance structures of adc-Salph(3-).

An EPR response corresponding to the open-shell complex **1**(PF_6) was not observed at room temperature or in the glassy frozen state (in dichloromethane) at 110 K. However, on measuring at 4.5 K, a rhombic signal was found in which the *g* components are highly affected by EPR line broadening.[12,13,23] The *g* values can be obtained from the simulated spectrum (Figure 3) which reveals a large *g*-anisotropy ($g_1-g_3\approx0.34$)[11] in comparison to reported organic-radical-bridged diruthenium species ($g_1-g_3<0.1$).[23] Therefore, the EPR data suggest that the SOMO has a predominant metal character in **1**(PF_6). The splitting of the *g* factors is very similar to that observed for symmetrical diruthenium systems with adc-R(2-) bridges, which have been described as delocalized mixed-valent ions.[11–13] This indicates that the SOMO has comparable contributions from metal and ligand orbitals in *both* the symmetrical and asymmetrical cases.

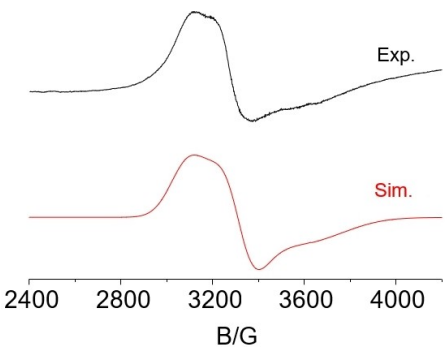

Figure 3. EPR spectrum of **1**(PF_6) in CH_2Cl_2 at 4.5 K with computer simulation ($g_1=2.175$, $g_2=2.025$, $g_3=1.84$).

Considering the structural asymmetry and the similarities with EPR features of related symmetrical systems, it can be proposed that the spin is distributed non-uniformly on both metal centres and the bridging ligand. Accordingly, a valence localized description Ru^{III}(μ-adc-Salph)$^{3-}Ru^{II}$ can be assumed for the asymmetrical mixed-valent complex **1**(PF_6).

The EPR data for the three compounds **1**(PF_6), **2**(PF_6) (Figure S3) and **3**(PF_6) are rather similar (Table 2) and do not strongly reflect the asymmetry of **1**(PF_6). In all instances there is considerably mixed metal/bridge contribution to the spin density.[11–13] Yet the DFT calculated spin densities for the trimethyl-terpyridine model suggest a highly asymmetric situation for **1**(PF_6), the unpaired electron residing mainly (0.63) at the phenolate-coordinated metal centre (Figure 4, Table S5). The chlororuthenium moieties are less easily oxidized, in agreement with the redox potential differences (Table 3, cf. below). The spin distribution in $\mathbf{3}^+$ is symmetrical with equal spin densities of 0.31 each at the metal centres.[17]

Table 2. EPR, NIR and N–N bond distance data for the complexes from Scheme 3.

	$\mathbf{1}^+$	$\mathbf{2}^+$	$\mathbf{3}^+$
g_1	2.175	2.217	2.19
g_2	2.025	2.057	1.95
g_3	1.840	1.092	1.74
g_{av}	2.047	2.059	1.96
$g_1-g_3=\Delta g$	0.335	0.315	0.45
λ_{max} (nm)	1464	1530	1645
d_{N-N} (Å)	1.427(6)	1.437(4)	1.392(6)

Research Article
doi.org/10.1002/ejic.202200319

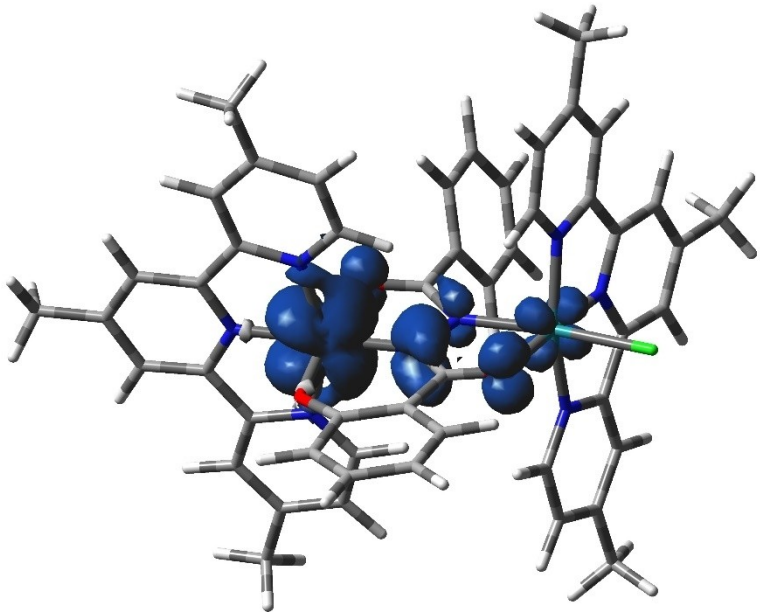

Figure 4. DFT calculated spin density for the trimethyl-terpyridine model of $\mathbf{1}^{+}$.

Table 3. Redox potentials from cyclic voltammetry.[a]

Complex	E^0 [V] $E_{1/2}$ (1)	$E_{1/2}$ (2)	K_c[b]
$\mathbf{1}^{n}$	−0.69	−0.11	$10^{9.8}$
$\mathbf{2}^{n}$	−0.42	0.08	$10^{8.5}$
$\mathbf{3}^{n}$	−0.77	−0.29	$10^{8.1}$

[a] Potentials in V vs $Fc^{+/0}$ in CH_2Cl_2/0.1 M Bu_4NPF_6 at room temperature. [b] $K_c = 10^{\Delta E/59\ mV} = [M^+]^2/[M][M^{2+}]$.

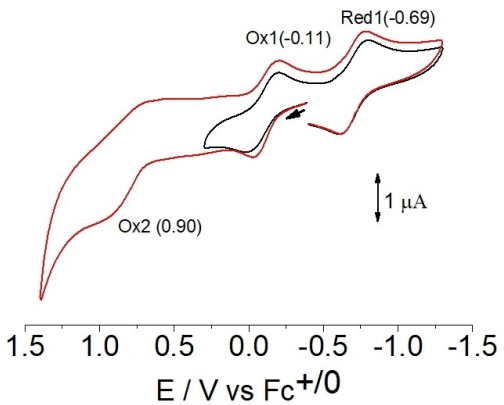

Figure 5. Cyclic voltammogram of $\mathbf{1}^{+}$ in CH_2Cl_2/0.1 M Bu_4NPF_6 at 100 mV scan rate.

Cyclic voltammetry

In its cyclic voltammogram the compound $\mathbf{1}(PF_6)$ exhibits one reversible oxidation at −0.11 V (vs. $Fc^{+/0}$) and one reversible reduction at −0.69 V. These redox processes are expected to be largely metal-based (Ru^{II}/Ru^{III} couples) as has been observed for previously reported dinuclear ruthenium complexes incorporating adc-R(2-) bridges.[11–13] In addition, an irreversible oxidation is observed at around 0.90 V. The voltammogram is shown in Figure 5, the redox potentials are listed in Table 3.

The importance of the comproportionation constant (K_c, Scheme 6, Table 3) in assessing metal-metal electronic coupling in symmetrical mixed-valence systems has been discussed.[1–4,24]

This electrochemical parameter also plays a vital role for unsymmetrical MV arrangements.[24–27] In symmetrical systems, the magnitude of the difference $\Delta E_{1/2}$ depends upon several factors such as the electrostatic interaction between two metal centres, the solvation energy of individual redox species and the charge delocalization in the MV intermediate.[24] In asymmetrical systems, an additional factor, the internal redox asymmetry, comes into play which is arising because of different coordinative situations of the redox-active metal sites. As a result, the K_c values of asymmetrical dinuclear species are always found to be higher than those of the structurally related symmetrical dimers.[25–28] Thus, it could be misleading to judge an asymmetrical mixed-valent system only by considering the K_c value.

The K_c values for $\mathbf{1}^{+}$, $\mathbf{2}^{+}$ (Figure S4) and $\mathbf{3}^{+}$ are rather similar (Table 3) with a slightly higher value for asymmetrical $\mathbf{1}^{+}$, suggesting relatively little redox asymmetry in the case of $\mathbf{1}(PF_6)$ from this kind of study.

UV-Vis-NIR spectroelectrochemistry

Spectroelectrochemical measurements for $\mathbf{1}(PF_6)$ were carried out in CH_2Cl_2/0.1 M Bu_4NPF_6 using an OTTLE cell.[29] Spectral changes in the UV-Vis-NIR region are shown in Figure 6 for both oxidation and reduction processes. Absorption values are listed

Research Article
doi.org/10.1002/ejic.202200319

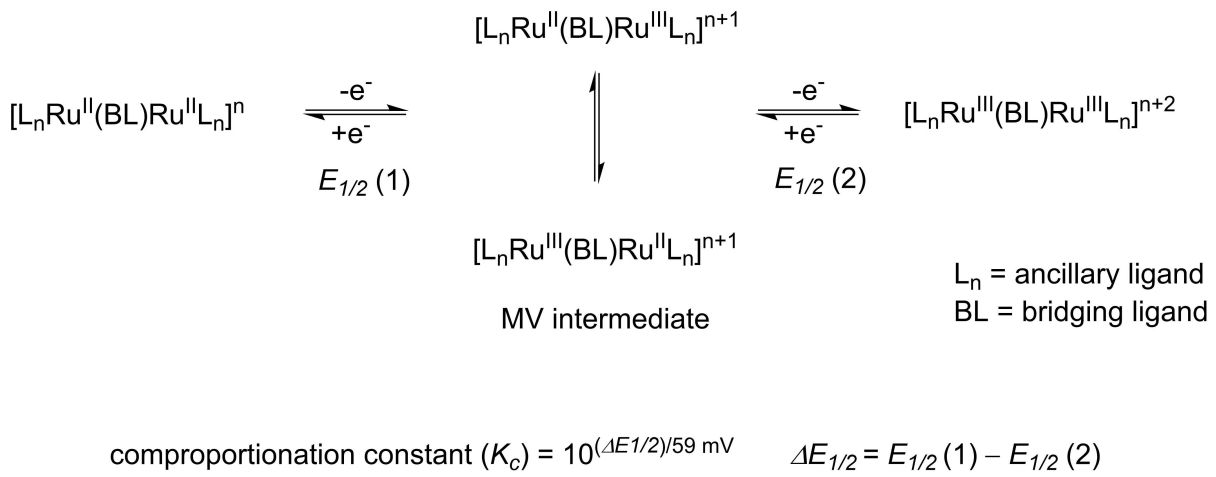

Scheme 6. Two-step redox scheme for diruthenium complexes incorporating a MV intermediate.

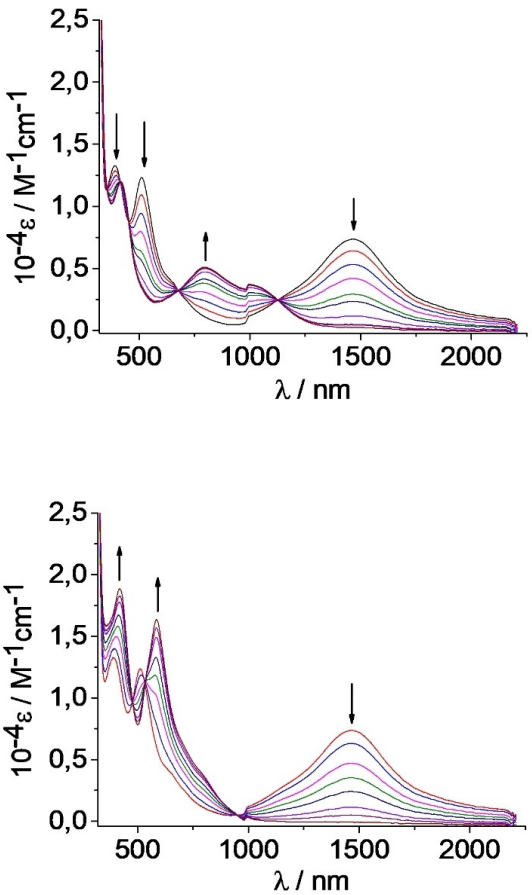

Figure 6. UV-Vis-NIR spectroelectrochemical responses on oxidation (top) and reduction (bottom) of $\mathbf{1}^{+}$ in CH_2Cl_2/0.1 M Bu_4NPF_6 (baseline correction applied below 1000 nm).

in Table 4, and comparison with the symmetrical systems $\mathbf{2}^{n}$ and $\mathbf{3}^{n}$ is presented in Figure S5 and Table 4.

The complex $\mathbf{1}(PF_6)$ exhibits an intense ($\varepsilon = 7000\ M^{-1}cm^{-1}$) absorption band in the NIR region at $\lambda_{max} = 1464$ nm which is attributed to an inter-valence charge-transfer (IVCT) transition from the Ru^{II}–Cl centre (molecular section B2, Scheme 4) to the bis-meridionally coordinated Ru^{III} centre (molecular part A). NIR absorptions around 1500 nm with considerable intensity ($\varepsilon \approx 5000\ M^{-1}cm^{-1}$)[1] have previously been found for cyclometalated[8] and non-cyclometalated[9] diruthenium complexes, including the symmetrical $\mathbf{2}^{+}$ and $\mathbf{3}^{+}$[17] (see Figure S5 for the new $\mathbf{2}(PF_6)$). Different coordination environments of two metal centres in a mixed-valent situation can create redox asymmetry to such an extent that it may cause only very weak interaction between metal centres, resulting in an absence of an IVCT band in the NIR region.[6] According to the Hush equation[1,30] which is applicable to a localized system (Class II system according to the Robin and Day classification), the half-bandwidth ($\Delta\nu_{1/2}$) of the IVCT band can be estimated by applying the following equations (i and ii) for a symmetrical (i) and an asymmetrical (ii) system, respectively.

$$\Delta\nu_{1/2}/cm^{-1} = [2.31 \times 10^{3}\ (\nu_{max}/cm^{-1})]^{1/2} \quad \text{(i)}$$

$$\Delta\nu_{1/2}/cm^{-1} = [2.31 \times 10^{3}\ \{(\nu_{max} - \Delta E_0)/cm^{-1}\}]^{1/2} \quad \text{(ii)}^{[7,30]}$$

In these equations, $\Delta\nu_{1/2}$ is the bandwidth at half height, ν_{max} the band energy maximum, and the quantity ΔE_0 is the potential difference between two redox isomers of the mixed-valent state (Scheme 6) which is non-zero for the asymmetrical case. As there is no straightforward way to calculate this quantity, we are assuming here that the ΔE_0 value for $\mathbf{1}(PF_6)$ is equal to the difference in redox potentials ($E_{1/2}(1)$, Scheme 6) of the structurally related symmetrical dinuclear compounds. Using this difference of 0.35 V (2823 cm^{-1}), the theoretical bandwidth is calculated to be 3042 cm^{-1}, which is somewhat larger than the observed value of 2228 cm^{-1}. Therefore, we assume that a strong metal/ligand/metal interaction is present in the asymmetrical mixed-valent complex $\mathbf{1}(PF_6)$.

The NIR band shown by $\mathbf{1}(PF_6)$ is absent in both one-electron reduced and one-electron oxidised states. A structured band forms at $\lambda_{max} = 795$ nm during oxidation to $\mathbf{1}^{2+}$ which can

Research Article
doi.org/10.1002/ejic.202200319

Table 4. Absorption values from UV-Vis-NIR spectroelectrochemistry.[a]

Compound	λ_{max}/nm (10^{-4} ε/$M^{-1}cm^{-1}$)
$\mathbf{1}^{2+}$	415(1.2), 795(0.5)
$\mathbf{1}^{+}$	390(1.3), 510(1.2), 680(sh), 1464(0.7)
1	420(1.9), 585(1.6), 815(sh)
$\mathbf{2}^{2+}$	408(0.7), 770(0.7)
$\mathbf{2}^{+}$	375(0.8), 490(0.8), 1530(0.9)
2	408(1.1), 536(1.0), 700sh, 780sh
$\mathbf{3}^{2+}$	406(1.4), 717(0.6), 926sh
$\mathbf{3}^{+}$	421(1.4), 541(1.6), 1645(0.7)
$\mathbf{3}^{0}$	439(2.4), 605(2.1), 798sh

[a] Data for $\mathbf{3}^{n}$ from ref. [17].

be attributed to a ligand-to-metal charge-transfer (LMCT) inside the Ru^{III}-(adc-Salph)$^{3-}$-Ru^{III} motif.

On reduction to $\mathbf{1}^{0}$, the terpyridine-based MLCT transitions (λ_{max} = 390, 510 nm)[18] are shifted to longer wavelengths (λ_{max} = 420, 585 nm). This behaviour indicates that the charge on the ruthenium centres has decreased on reduction. The reduced species also exhibits a shoulder at around 815 nm, which can be attributed to a ligand-to-ligand charge transfer transition (LLCT). The complexes $\mathbf{2}^{n}$ exhibit similar spectroelectrochemical behaviour as other symmetric dinuclear complexes with adc-R bridging ligands.[11–13]

Simulated absorption spectra of the trimethyl-terpyridine-modified models of $\mathbf{1}^{+}$ and the reduced species $\mathbf{1}^{0}$ are depicted in Figure S7, indicating that the TD DFT calculations qualitatively reproduce the UV-Vis-NIR spectra of $\mathbf{1}^{+}$ and its reduction product. The absorption of the cation in the near IR region around 1500 nm corresponds to calculated transitions at 1218 and 1003 nm. These intense transitions formed by combined βHOMO→βLUMO, βHOMO-1→βLUMO and βHOMO-3→βLUMO excitations (Table S6 and Figures S6 and S7) can be described as intervalence features with an admixture of IL (intra-ligand) and metal centered transitions. In the course of the reduction an electron is accepted into the βLUMO forming a neutral diruthenium(II) closed shell system. TD DFT calculations of the reduced model species indicate that the transition in the NIR diminishes (Figures 6 and S7, Table S6) and the feature in the visible region is shifted to longer wavelength.

Conclusion and outlook

This article contains a comparative description of an asymmetrical system $\mathbf{1}^{n}$ and related symmetrical paramagnetic diruthenium complexes ($\mathbf{2}^{n}$, $\mathbf{3}^{n}$) with the following remarkable results:

i) A new asymmetrical diruthenium complex **1**(PF_6) with a potentially redox-active bridging chelate ligand (bidentate and tridentate) has been synthesized.
ii) Structural characterization of the largely mixed-valent cation $\mathbf{1}^{+}$ has revealed the asymmetrical nature of the metal/ligand interface and of the bridge adc-Salph(3-).
iii) A strong NIR absorption at λ_{max} = 1416 nm (ε = 7000 $M^{-1}cm^{-1}$) has been observed for $\mathbf{1}^{+}$.

The electrochemical results for asymmetrical $\mathbf{1}^{+}$ and the related symmetrical analogues $\mathbf{2}^{+}$ and $\mathbf{3}^{+}$ (Scheme 3) with delocalized bonding and spin distribution over d/π/d orbitals reflect the strong donating ability of the coordinated phenolate moiety in comparison to the chloride ligand. Considering the electrochemical results in comparison with experimental and calculated structural and EPR data for a model compound, the electronic situation of $\mathbf{1}^{+}$ may be formulated as [(trpy*)Ru^{III}(adc-Salph)$^{3-}$$Ru^{II}$(trpy*)Cl]$^{+}$ where bis-meridionally coordinated ruthenium bears most of the spin density. The intense IVCT band in the NIR region reveals the capability of an asymmetrical ligand such as adc-Salph(3-) to mediate electron transfer between the Ru centres in respective molecular sections (Scheme 7).

Generalizing, the classical molecule-bridged diruthenium(III,II) arrangement based on the Creutz-Taube ion[1–3] continues to offer interesting features after modifying the ligand set. Aspects of symmetry[31a] may be considered, and the demonstrated ambiguity[3,11] of mixed-valency[31b] and radical bridging[31c] has received renewed interest recently in connection with lanthanide complexes and molecular magnetism.[31b,c]

Experimental Section

Instrumentation. A Bruker EMX system was used for X band (9.5 GHz) EPR spectroscopy. ^{1}H NMR spectra were taken at 298 K on an AV 250 spectrometer from Bruker. Electron spray mass spectrometry was recorded on a Bruker Daltronics Microtof Q instrument. Cyclic voltammetry was performed with a PAR 273 potentiostat using a three electrode set-up (Pt working electrode, Pt counter electrode, Ag wire pseudoreference electrode). The $Fc^{+/0}$ couple served as an internal reference. A J&M TIDAS spectrophotometer was used for UV-Vis-NIR spectroelectrochemical measurements, by incorporating an optically transparent thin-layer electrochemical (OTTLE) cell.[29]

Materials. Symmetrical and asymmetrical 1,2-dicarbonylhydrazine ligands H_2(adc-Ph)[19] and H_3(adc-Salph)[14] and the metal precursor complex *mer*-[Ru(trpy*)Cl_3][18] were prepared following literature procedures. All other chemicals and reagents were of reagent grade and used without further purification. Dry HPLC grade solvents were used for spectroscopic and electrochemical measurements. Reactions related to ruthenium complexes were performed under an argon atmosphere.

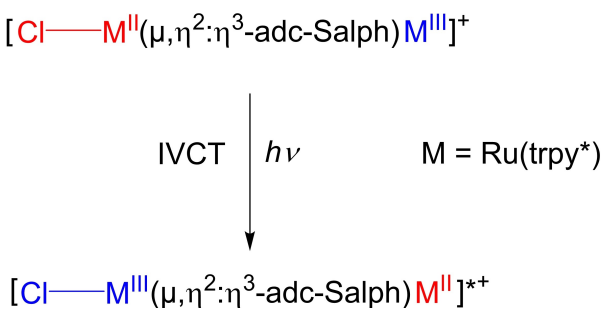

Scheme 7. Assignment of NIR absorption of $\mathbf{1}^{+}$ as IVCT transition.

Syntheses. [{Ru(trpy*)}$_2$(μ-adc-Salph)Cl](PF$_6$), 1(PF$_6$). To a mixture of 100 mg (0.16 mmol) of *mer*-[Ru(trpy*)Cl$_3$] and of 20 mg (0.08 mmol) H_3adc-Salph, dissolved in 20 ml of EtOH, a few drops of Et_3N were added and the mixture was heated to reflux for 15 h. The initial greenish yellow solution gradually changed to deep purple. After cooling to room temperature 0.5 g of KPF_6 dissolved in 25 ml water were added and the precipitate thus obtained was filtered off and washed with cold water and purified on a neutral Al_2O_3 column. With dichloromethane/acetone (10:1) solvent mixture a purple solution corresponding to [{Ru(trpy*)Cl}$_2$(μ-adc-Ph)](PF$_6$) was eluted. The solvent was removed under reduced pressure to obtain a deep purple coloured product. Yield: 40 mg (34%); Anal. Calcd. (Found) for $C_{68}H_{79}ClF_6N_8O_3PRu_2$ (1438.96 g/mol): C, 56.76 (55.62) H, 5.53 (5.50) N, 7.79 (7.65%); m/z = 1294.4 (M-PF$_6$); ^{1}H NMR (250 MHz, $(CD_3)_2CO$) δ (ppm) = 14.7 (s, 3H), 11.6 (2 s, 2H), 9.9 (s, 3H), 8.4 (s, 2H), 6.4 (s, 3H), 6.2 (s, 5H), 5.8 (s, 4H), 1.8 (s, 18H), 1.43 (s, 9H), 1.41 (s, 18H), 1.2 (s, 9H). See main text for NMR discussion.

[{Ru(trpy*)Cl}$_2$(μ-adc-Ph)](PF$_6$), 2(PF$_6$). To a mixture of 100 mg (0.16 mmol) of *mer*-[Ru(trpy*)Cl$_3$] and an amount of 20 mg (0.08 mmol) H_2adc-Ph,[19] dissolved in 20 ml of EtOH, a few drops of Et_3N were added and the mixture was heated to reflux for 15 h. The initial greenish yellow solution gradually changed to deep purple. After cooling to room temperature 0.5 g of KPF_6 dissolved in 25 ml water were added and the precipitate thus obtained was filtered off and washed with cold water and purified on a neutral Al_2O_3 column. With dichloromethane/acetone (10:1) solvent mixture a purple solution corresponding to [{Ru(trpy*)Cl}$_2$(μ-adc-Ph)](PF$_6$) was eluted. The solvent was removed under reduced pressure to obtain a deep purple coloured product. Yield: 55 mg (46%); Anal. Calcd. (Found) for $C_{68}H_{80}Cl_2F_6N_8O_2PRu_2$ (1459.42 g/mol): C, 55.96 (55.67) H, 5.53 (5.88) N, 7.68 (7.70%) ; m/z = 1314.3 (M-PF$_6$); ^{1}H NMR (250 MHz, $(CD_3)_2CO$): δ (ppm) = 20.7 (s, 4H), 13.5 (s, 4H), 9.3 (b, 4H) 8.8 (b, 6H), 6.3 (s, 4H), 5.3 (s, 4H), 1.85 (s, 36H), 1.49 (s, 18H). See main text for NMR discussion.

X-ray crystallography. Suitable single crystals for X-ray diffraction were grown by slow diffusion of hexane into dichloromethane or l,2-dichloroethane solutions of **1**(PF$_6$) or **2**(PF$_6$), respectively.

X-ray diffraction data were collected at 100 K using a Bruker Kappa APEX II Duo diffractometer with a graphite monochromator. The radiation used was MoKα (λ = 0.71073 Å) or CuKα (λ = 1.54178 Å). The structures were solved using Olex2[32] with the SHELXS structure solution program using Direct Methods and refined with the SHELXL[33] refinement package using Least Squares minimization. Absorption corrections were done by the multiscan technique or by numeric means (see Supporting Information). All non-hydrogen atoms were refined anisotropically, hydrogen atoms were included in the refinement process as per the riding model.

1(PF$_6$)×4CH_2Cl_2 crystallizes in space group *P*2$_1$/*c*. Highly disordered solvent molecules were squeezed by PLATON/SQUEEZE procedure[34] to obtain better overall standard deviations of the geometry parameters of the actual target molecules. Some *tert*-butyl groups showed disorder. **2**(PF$_6$)×3 $C_2H_4Cl_2$ crystallizes in the *Pbca* space group and the squeeze treatment was performed to remove 2 solvent molecules.

DFT calculations. The electronic structures of the asymmetric complexes [(trpy')Ru(μ-adc-Ph)RuCl(trpy')]^n **1**^{n}, n = 0,1), where the bulky *tert*-Bu substituents on trpy ligands (trpy*) were replaced by methyls (trpy'), were calculated by density functional theory (DFT) methods using the Gaussian 16[35] (G16) program package. Within G16 calculations the Stuttgart/Dresden quasirelativistic effective core pseudopotentials and the corresponding optimized set of basis functions for Ru[36,37] and 6-311G(d) polarized triple-ζ basis sets[38] for the remaining atoms were used. G16 calculations employed the hybrid Perdew, Burke, Ernzerhof[39,40] exchange and correlation functional (PBE0). The solvent was described by the polarizable calculation model (PCM).[41] Geometry optimizations were performed both in vacuo and with PCM correction. Geometry optimizations were followed by vibrational analysis, for optimized structures no imaginary frequencies were found. Electronic excitations were calculated by time dependent DFT (TD DFT) method at optimized geometries. For analysis of singlet diradicals, a symmetry breaking approach (SB-UKS)[42,43] within DFT was used.

Supporting Information

The Supporting Information is available free of charge.

Deposition Numbers 2150605 (for **1**(PF$_6$)×$C_2H_4Cl_2$) and 2150606 (for **2**(PF$_6$)) contain the supplementary crystallographic data for this paper. These data are provided free of charge by the joint Cambridge Crystallographic Data Centre and Fachinformationszentrum Karlsruhe Access Structures service www.ccdc.cam.ac.uk/structures.

Acknowledgements

The authors acknowledge support by the state of Baden-Württemberg. The contributions by Dipl.-Chem. Angela Winkelmann and Dr. Wolfgang Frey are gratefully acknowledged. S. Z. acknowledges support by the Czech Science Foundation (GAČR, Grant No. 21-05180S). Open Access funding enabled and organized by Projekt DEAL.

Conflict of Interest

The authors declare no conflict of interest.

Data Availability Statement

The data that support the findings of this study are openly available in The Cambridge Crystallographic Data Centre, 12 Union Road, Cambridge CB2 1EZ, UK at www.ccdc.cam.ac.uk/data_request/cif, reference number 2150605.

Keywords: Mixed valence · Radical complexes · Redox series · Ruthenium compounds · Symmetry

[1] C. Creutz, *Prog. Inorg. Chem.* **1983**, *30*, 1–73.
[2] W. Kaim, W. Bruns, J. Poppe, V. Kasack, *J. Mol. Struct.* **1993**, *292*, 221–228.
[3] a) W. Kaim, A. Klein, M. Glöckle, *Acc. Chem. Res.* **2000**, *33*, 755–763; b) W. Kaim, G. K. Lahiri, *Angew. Chem. Int. Ed.* **2007**, *46*, 1778–1796; *Angew. Chem.* **2007**, *119*, 1808–1828.
[4] W. Kaim, B. Sarkar, *Coord. Chem. Rev.* **2007**, *251*, 584–594.
[5] Y. W. Zhong, Z. L. Gong, J. Y. Shao, J. Yao, *Coord. Chem. Rev.* **2016**, *312*, 22–40.
[6] A. Mandal, M. A. Hoque, A. Grupp, A. Paretzki, W. Kaim, G. K. Lahiri, *Inorg. Chem.* **2016**, *55*, 2146–2156.
[7] R. C. Rocha, H. E. Toma, *Inorg. Chim. Acta* **2000**, *310*, 65–80.
[8] W.-W. Yang, J. Yao, Y.-W. Zhong, *Organometallics* **2012**, *31*, 8577–8583.

[9] G. E. Pieslinger, B. M. Aramburu-Trošelj, A. Cadranel, L. M. Baraldo, *Inorg. Chem.* **2014**, *53*, 8221–8229.
[10] W. Kaim, *Coord. Chem. Rev.* **2011**, *255*, 2503–2513.
[11] V. Kasack, W. Kaim, H. Binder, J. Jordanov, E. Roth, *Inorg. Chem.* **1995**, *34*, 1924–1933.
[12] W. Kaim, V. Kasack, *Inorg. Chem.* **1990**, *29*, 4696–4699.
[13] a) R. Jana, B. Sarkar, D. Bubrin, J. Fiedler, W. Kaim, *Inorg. Chem. Commun.* **2010**, *13*, 1160–1162; b) S. Roy, B. Sarkar, H.-G. Imrich, J. Fiedler, S. Záliš, R. Jimenez-Aparicio, F. A. Urbanos, S. M. Mobin, G. K. Lahiri, W. Kaim, *Inorg. Chem.* **2012**, *51*, 9273–9281.
[14] a) S.-X. Liu, S. Lin, B. Z. Lin, C.-C. Lin, J.-Q. Huang, *Angew. Chem. Int. Ed.* **2001**, *40*, 1084–1087; *Angew. Chem.* **2001**, *113*, 1118–1121; b) A. Majumder, S. Goswami, S. R. Batten, M. Salah El Fallah, J. Ribas, S. Mitra, *Inorg. Chim. Acta* **2006**, *359*, 2375–2382.
[15] M. Sutradhar, M. V. Kirillova, M. F. C. Guedes da Silva, L. M. D. R. S. Martins, A. J. L. Pombeiro, *Inorg. Chem.* **2012**, *51*, 11229–11231.
[16] a) W. Luo, X.-T. Wang, X.-G. Meng, G.-Z. Cheng, Z.-P. Ji, *Polyhedron* **2009**, *28*, 300–306; b) W. Luo, X.-G. Meng, J.-F. Xiang, Y. Duan, G.-Z. Cheng, Z.-P. Ji, *Inorg. Chim. Acta* **2008**, *361*, 2667–2676; c) W. Luo, X.-T. Wang, X.-G. Meng, G.-Z. Cheng, Z.-P. Ji, *Inorg. Chem. Commun.* **2008**, *11*, 1044–1047.
[17] S. Mondal, B. Schwederski, W. Frey, J. Fiedler, S. Záliš, W. Kaim, *Inorg. Chem.* **2018**, *57*, 3983–3992.
[18] T. B. Hadda, H. L. Bozec, *Inorg. Chim. Acta* **1993**, *204*, 103–107.
[19] R. N. Butler, H. N. Hanniffy, J. C. Stephens, L. A. Burke, *J. Org. Chem.* **2008**, *73*, 1354–1364.
[20] S. Roy, M. Sieger, P. Singh, M. Niemeyer, J. Fiedler, C. Duboc, W. Kaim, *Inorg. Chim. Acta* **2008**, *361*, 1699–1704.
[21] a) A. Das, T. M. Scherer, S. M. Mobin, W. Kaim, G. K. Lahiri, *Chem. Eur. J.* **2012**, *18*, 11007–11018; b) W. Kaim, *Coord. Chem. Rev.* **2001**, *219–221*, 463–488.
[22] R. C. Rocha, F. N. Rein, H. Jude, A. P. Shreve, J. J. Concepcion, T. J. Meyer, *Angew. Chem. Int. Ed.* **2008**, *47*, 503–506; *Angew. Chem.* **2008**, *120*, 513–516.
[23] W. Kaim, in *Electron Transfer in Chemistry* (Ed.: V. Balzani), Wiley-VCH, Weinheim, **2001**, vol. 2, pp. 976–1002.
[24] R. D. Crutchley, *Adv. Inorg. Chem.* **1994**, *41*, 273–325.
[25] R. Hage, J. G. Haasnoot, H. A. Nieuwenhuis, J. Reedijk, D. J. A. De Ridder, J. G. Vos, *J. Am. Chem. Soc.* **1990**, *112*, 9245–9251.
[26] K. A. Goldsby, T. J. Meyer, *Inorg. Chem.* **1984**, *23*, 3002–3010.
[27] J. Otsuki, A. Imai, K. Sato, D.-M. Li, M. Hosoda, M. Owa, T. Akasaka, I. Yoshikawa, K. Araki, T. Suenobu, S. Fukuzumi, *Chem. Eur. J.* **2008**, *14*, 2709–2718.
[28] W. Y. Yu, M. Meng, H. Lei, X. D. He, C. Y. Liu, *J. Phys. Chem. C* **2016**, *120*, 12411–12422.
[29] M. Krejčík, M. Daněk, F. Hartl, *J. Electroanal. Chem.* **1991**, *317*, 179–187.
[30] a) N. S. Hush, *Coord. Chem. Rev.* **1985**, *64*, 135–157; b) N. S. Hush, *Prog. Inorg. Chem.* **1967**, *8*, 391–444.
[31] a) J. C. Salsman, C. P. Kubiak, T. Ito, *J. Am. Chem. Soc.* **2005**, *127*, 2382–2383; b) C. A. Gould, K. R. McClain, D. Reta, J. G. C. Kragskow, D. A. Marchiori, E. Lachman, E.-S. Choi, J. G. Analytis, R. D. Britt, N. F. Chilton, B. G. Harvey, J. R. Long, *Science* **2022**, *375*, 198–202; c) S. Demir, M. I. Gonzalez, L. E. Darago, W. J. Evans, J. R. Long, *Nat. Commun.* **2017**, *2144*, 1–9.
[32] O. V. Dolomanov, L. J. Bourhis, R. J. Gildea, J. A. K. Howard, H. Puschmann, *J. Appl. Crystallogr.* **2009**, *42*, 339–341.
[33] G. M. Sheldrick, *Acta Crystallogr.* **2008**, *A64*, 112–122.
[34] A. L. Spek, *Acta Crystallogr. Sect. D* **2009**, *65*, 148–155.
[35] M. J. Frisch, G. W. Trucks, H. B. Schlegel, G. E. Scuseria, M. A. Robb, J. R. Cheeseman, G. Scalmani, V. Barone, G. A. Petersson, H. Nakatsuji, X. Li, M. Caricato, A. V. Marenich, J. Bloino, B. G. Janesko, R. Gomperts, B. Mennucci, H. P. Hratchian, J. V. Ortiz, A. F. Izmaylov, J. L. Sonnenberg, D. Williams-Young, F. Ding, F. Lipparini, F. Egidi, J. Goings, B. Peng, A. Petrone, T. Henderson, D. Ranasinghe, V. G. Zakrzewski, J. Gao, N. Rega, G. Zheng, W. Liang, M. Hada, M. Ehara, K. Toyota, R. Fukuda, J. Hasegawa, M. Ishida, T. Nakajima, Y. Honda, O. Kitao, H. Nakai, T. Vreven, K. Throssell, J. A. Montgomery, J. E. Peralta, F. Ogliaro, M. J. Bearpark, J. J. Heyd, E. N. Brothers, K. N. Kudin, V. N. Staroverov, T. A. Keith, R. Kobayashi, J. Normand, K. Raghavachari, A. P. Rendell, J. C. Burant, S. S. Iyengar, J. Tomasi, M. Cossi, J. M. Millam, M. Klene, C. Adamo, R. Cammi, J. W. Ochterski, R. L. Martin, K. Morokuma, O. Farkas, J. B. Foresman, D. J. Fox, *Gaussian16, Revision A.03*, Gaussian, Inc.: Wallingford, CT, 2016.
[36] D. Andrae, U. Haeussermann, M. Dolg, H. Stoll, H. Preuss, *Theor. Chim. Acta* **1990**, *77*, 123–141.
[37] J. M. L. Martin, A. J. Sundermann, *Chem. Phys.* **2001**, *114*, 3408–3420.
[38] L. A. Curtiss, M. P. McGrath, J.-P. Blaudeau, N. E. Davis, R. C. Binning Jr., L. Radom, *J. Chem. Phys.* **1995**, *103*, 6104–6113.
[39] J. P. Perdew, K. Burke, M. Ernzerhof, *Phys. Rev. Lett.* **1996**, *77*, 3865–3868.
[40] C. Adamo, V. Barone, *J. Chem. Phys.* **1999**, *110*, 6158–6170.
[41] M. Cossi, N. Rega, G. Scalmani, V. Barone, *J. Comput. Chem.* **2003**, *24*, 669–681.
[42] F. Neese, *J. Phys. Chem. Solids* **2004**, *65*, 781–785.
[43] L. Noodleman, *J. Chem. Phys.* **1981**, *74*, 5737–5743.

Manuscript received: May 17, 2022
Revised manuscript received: June 1, 2022
Accepted manuscript online: June 3, 2022